IUST
Iran University of Science and Technology

Iranian Journal of Electrical and Electronic Engineering

Journal Homepage: ijeee.iust.ac.ir

Convolutional Neural Network Classification using Three Cepstrums Combinations with Time, Time Derivative and Reassigned STFT of Doppler Signatures from Radar Human Locomotion

D.Yessad*(C.A.)

Abstract: This paper introduces the CTDRCepstrum, a novel feature extraction technique designed to differentiate various human activities using Doppler radar classification. Real data were collected from a Doppler radar system, capturing nine return echoes while monitoring three distinct human activities: walking, fast walking, and running. These activities were performed by three subjects, either individually or in pairs. We focus on analyzing the Doppler signatures using time-frequency reassignment, emphasizing its advantages such as improved component separability. The proposed CTDRCepstrum explores different window functions, transforming each echo signal into three forms of Short-Time Fourier Transform reassignments (RSTFT): time RSTFT (TSTFT), time derivative RSTFT (TDSTFT), and reassigned STFT (RSTFT). A convolutional neural network (CNN) model was then trained using the feature vector, which is generated by combining the cepstral analysis results of each RSTFT form. Experimental results demonstrate the effectiveness of the proposed method, achieving a remarkable classification accuracy of 99.83% by using the Bartlett-Hanning window to extract key features from real-time Doppler radar data of moving targets.

Keywords: Doppler signature, STFT reassignment, Barttlet-Hanning window, CNN model, Radar target classification.

1 Introduction

THE classification of moving targets through Doppler radar signatures of human movement is imperative for all applications in the fields of security, civil utilization, military intelligence for ground surveillance, and police radar detection systems [1], [2], [3].and [4]. To understand Doppler signatures, it is necessary to return to the fundamentals of electromagnetic waves, particularly in the context of radar range returns. The sound signals received by the Doppler radar from the target are non-stationary and nonlinear. An effective approach to analyzing such signals involves time-frequency methods [5], [6], [7], and [8]. For instance, the widely used Short Time Fourier Transform (STFT) decomposes a signal into overlapping segments of equal size and applies the Fourier transform independently to each segment. However, the STFT presents a low energy localization in the time-frequency plane. An effective approach to enhance this is by applying the reassignment method, introduced in 1976, to sharpen the time-frequency representation [9]. Although this technique was initially little known and rarely used in the literature, it re-emerged nineteen years later with the reassignment method [10], which introduced a generalized approach applicable to any bilinear time-frequency or time-scale distribution. Over the years, it was further refined with algorithmic advancements and applied to various fields [11], [12], [13], [14], [15], [16],

Iranian Journal of Electrical & Electronic Engineering, 2024.
Paper first received 22 October 2024 and accepted 29 December 2024.
* The author is with the Department of Electromechanical and Mechanical Engineering, Institute of Science and Technology, University Center Abdelhafid Boussouf of Mila. Mila 43000, Algeria.
E-mail: d.yessad@centre-univ-mila.dz.
Corresponding Author: D.Yessad.

[17], [18], [19], and [20]. The concept of reassignment has recently been introduced under various names, including the reassignment method, remapping, time-frequency reassignment, and modified moving-window method [21], [22], [23]. The Time-Frequency Reassignment (TFR) method addresses the issue of low energy localization [24], [25], [26], [27], [28], enhancing the clarity and interpretability of the spectrogram.

The CTDRCepstrum is an advanced feature extraction method introduced in this study. This algorithm combines three distinct cepstrums, each derived from different variations of the Short-Time Fourier Transform reassignments (RSTFT): the standard STFT reassignment (RSTFT), the time-ramped RSTFT (TSTFT), and the time-derivative RSTFT (TDSTFT). The extracted features are then input into the CNN classification process. Simulation results demonstrate the efficiency of the proposed algorithm, highlighting its effectiveness in extracting Doppler signature features.

This work presents real data acquired from a radar Doppler system in Section 2. Section 3 reviews the theory of time-frequency reassignment and provides a detailed explanation of the proposed method. An overview of convolutional neural networks (CNNs) is presented in Section 4. Section 5 covers the results, discussion, and implementation details, while Section 6 concludes the work with a summary of the findings.

2 Doppler Database

Doppler data were captured from low-resolution ground-surveillance radar recordings. The data acquisition sensor is an impulse Doppler radar operating at limited elevation angles of approximately 270°, with an azimuth sweep of 30°, at an emission power of 100 mW. It operates at a frequency of 9.72 GHz. Echoes were collected for nine scenarios involving radar targets consisting of one, two, or three individuals. In each scenario, one target echo was recorded at a time, corresponding to three different human activities: walking, fast walking, and running. Each scenario was recorded at least twice, with a duration of five seconds per recording. Fig. 1 shows the plot of nine echoes returned from one, two, and three persons. Each target class exhibits distinct time-frequency characteristics, which can be exploited for classification purposes.

3 STFT Reassignment with the New CTDRCepstrum Technique

The short time Fourier transform (STFT) of time domain Doppler signal $x(t)$ is typically defined using an analysis window $h(t)$ as follows [29]:

$$STFT_h(t,w) = \int_{-\infty}^{+\infty} x(\tau)h^*(\tau - t)e^{-jw\tau}d\tau \quad (1)$$

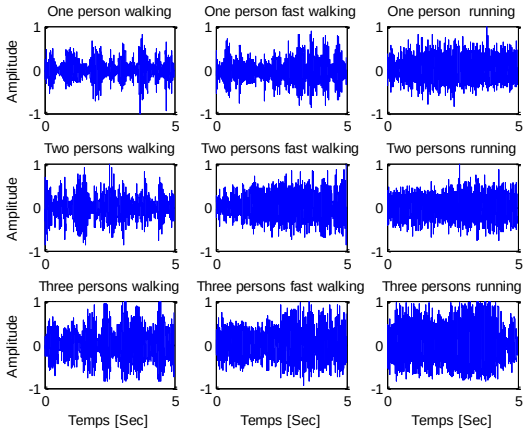

Fig. 1 Nine Doppler Echoes from Radar-Detected Human Movement Targets.

Where $*$ signifies the complex conjugate. Squared absolute value of the STFT denote $STFT_h$ transform usually referred as a spectrogram:

$$S_h(t,w) = |STFT_h(t,w)|^2 \quad (2)$$

The $STFT_h$ polar form can be expressed as:

$$STFT_h(t,w) = M(t,w)e^{j\emptyset(t,w)} \quad (3)$$

Where $M(t,w)$ is magnitude and $\emptyset(t,w)$ is the phase of $STFT_h$ defined as a function of continuous time t and angular frequency w. The reassigned time-frequency coordinates $(\hat{t},\hat{w})$ may be calculated from the derivatives of the spectral phase as follows:

$$\hat{t}(t,w) = -\frac{\vartheta\emptyset(t,w)}{\vartheta w} \quad (4)$$

$$\hat{w}(t,w) = w + \frac{\vartheta\emptyset(t,w)}{\vartheta t} \quad (5)$$

The time and frequency reassignment operators, as defined in equations (2) and (3), cannot be directly computed. That is why this representation has not been exploited much. According to [10] and [20] the reassigned transformation reallocates spectral energy from the coordinate (t,w) into a new time-frequency coordinate $(\hat{t},\hat{w})$, which reflects the distribution of energy in the analyzed signal in a more accurate way. The reassignment operations can be carried out when two helper windows are utilized, the time and frequency reassignment vectors can be formulated as:

$$\hat{t}(t,w) = t - \Re\left\{\frac{STFT_{th}(t,w).STFT_h^*(t,w)}{|STFT_h(t,w)|^2}\right\} \quad (6)$$

$$\hat{w}(t,w) = w - \Im\left\{\frac{STFT_{dh}(t,w).STFT_h^*(t,w)}{|STFT_h(t,w)|^2}\right\} \quad (7)$$

Where $STFT_h$ is the complex STFT calculated using an analysis window $h(t)$. $STFT_{th}$ is the complex STFT calculated using time ramped window $th = t.h(t)$, which is a time weighted version of the original window $h(t)$ multiplied by the time offset from the window center. $STFT_{dh}$ is the complex STFT calculated using time derivative window $dh = \frac{d}{dt}h(t)$, which is

equivalent to weighting the Fourier transform of the original window with a frequency ramp. The last step of the reassignment consists in moving the values of the spectrogram to obtain a sharpened representation, expressed as:

$$RS_h(t,w) = \iint |STFT_h(\tau,\Omega)|^2 \delta\big(t - \hat{t}(\tau,\Omega)\big)\delta(w - \hat{w}(\tau,\Omega)\big)d\tau d\Omega \quad (8)$$

Where $\delta(t)$ is the Dirac distribution.

Since there are different kinds of windows, the choice of a windowing function can strongly affect the quality of the overall results. The CTDRCepstrum technique presented here is computed at any time frequency coordinate. Classical windows such as Bartlett, Kaiser and Flattop are exploited for constructing both time weighted and time derivative windowing functions.

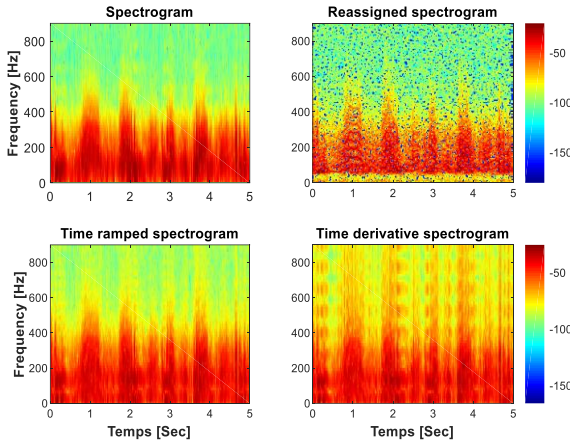

Fig. 2 Spectrograms based original STFT, RSTFT, TSTFT and TDSTFT.

Fig. 2 presents four spectrogram types from different STFT reassignment methods. It includes: (a) the original STFT using a standard window, and three reassignment variations: (b) Reassigned STFT (RSTFT), (c) Time STFT (TSTFT), and (d) Time Derivative STFT (TDSTFT). All spectrograms are generated using the Bartlett-Hanning window.

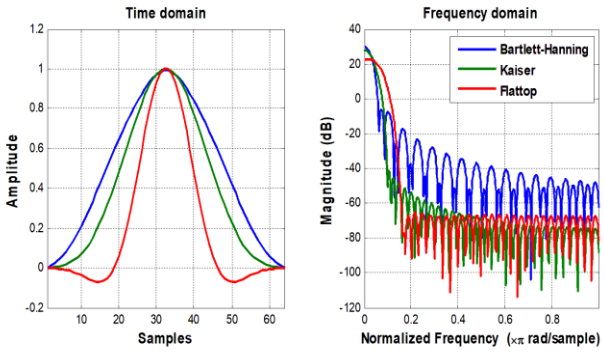

Fig. 3 Temporal and frequency domain plots of the length 64 based Bartlett-Hanning, Kaiser and Flattop windows.

Fig. 3 shows the time-domain and frequency-domain magnitude responses for the Bartlett-Hanning, Kaiser, and Flattop windows, each with a length of 64. **Fig. 4** illustrates the corresponding auxiliary time windows for these same window functions. **Fig. 5** presents the auxiliary time derivatives for the Bartlett-Hanning, Kaiser, and Flattop windows.

Fig. 3 Detailed comparison of time-domain and frequency-domain characteristics for the Bartlett-Hanning, Kaiser, and Flattop windows (window length = 64) in the context of their impact on the proposed technique. In the time domain, the Bartlett-Hanning window demonstrates the broadest shape, followed by the Kaiser window, with the Flattop window being the narrowest. This influences the temporal resolution of the technique, as wider windows allow better averaging but may reduce time localization. In the frequency domain, the trade-off between main lobe width and side lobes is crucial for spectral analysis. The Bartlett-Hanning window exhibits the narrowest main lobe, providing enhanced frequency resolution, whereas the Flattop window has the widest main lobe, which reduces frequency resolution but achieves superior side lobes. Kaiser balances these trade-offs, featuring a moderately narrow main lobe and reduced side lobes, with its first side lobe being the lowest among the three. For distant side lobes, Kaiser and Flattop outperform Bartlett-Hanning, making them more effective in suppressing spectral leakage in the technique. These properties play a pivotal role in optimizing the performance of the proposed method by addressing the balance between time and frequency localization and mitigating spectral artifacts.

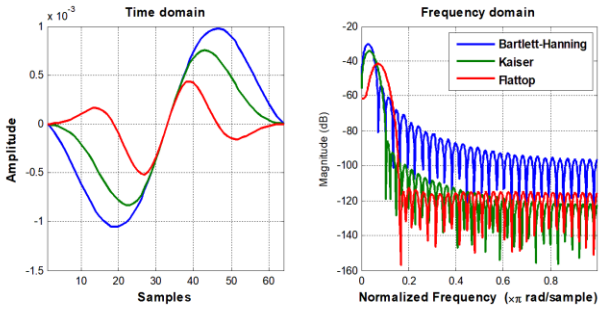

Fig. 4 Temporal and frequency domain plots of time ramped window based Bartlett-Hanning, Kaiser and Flattop windows.

Fig. 4 illustrates a comparative plot of Bartlett-Hanning, Kaiser, and Flattop time-ramped windows, highlighting their impact on side lobe behavior. It is observed that the side lobe magnitude decreases with increasing frequency, demonstrating the effectiveness of combining time-ramped functions with classical windows. This combination significantly enhances side lobe attenuation, reducing spectral leakage and

improving the precision of the proposed technique.

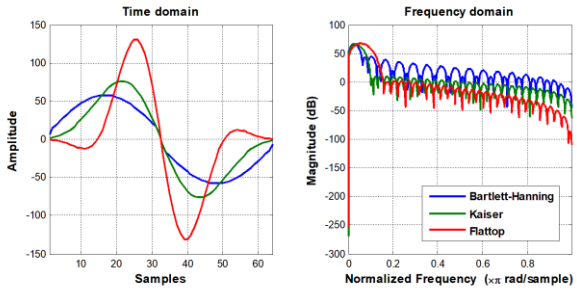

Fig. 5 Temporal and frequency plots of time derivative window based Bartlett-Hanning, Kaiser and Flattop windows.

In Fig. 5, the auxiliary time derivative windows of Bartlett-Hanning, Kaiser, and Flattop show significantly reduced side lobe peaks compared to their standard windows. However, their side lobe peaks remain slightly higher than those of the time-ramped windows, which demonstrate the best overall magnitude response. These results highlight the superiority of time-ramped windows in achieving enhanced side lobe attenuation while maintaining frequency resolution. This balance between side lobe and spectral resolution is crucial for applications demanding precise spectral analysis. By minimizing spectral leakage and improving signal clarity, time-ramped windows prove to be the optimal choice for the proposed methodology, ensuring robust performance in critical analysis tasks.

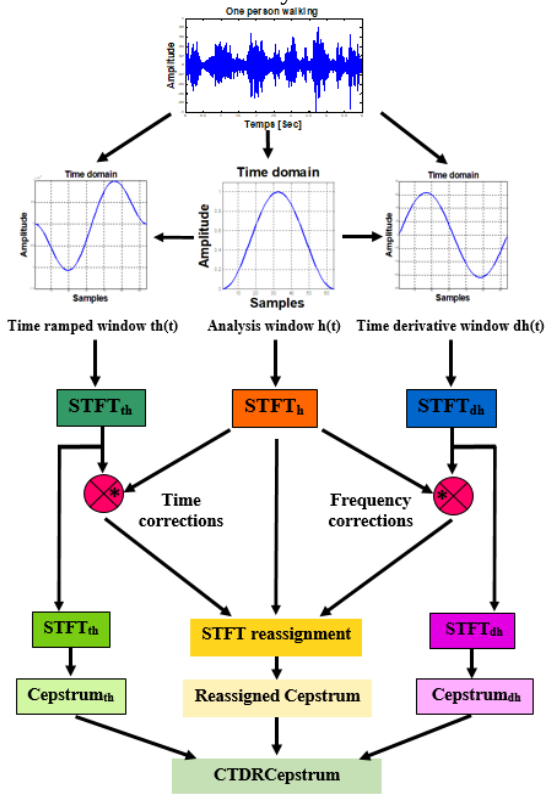

Fig. 6 CTDRCepstrum feature extraction technique.

To improve the accuracy of Doppler target classification, the CTDRCepstrum was calculated using three distinct Short-Time Fourier Transforms Reassignment (RSTFTs): RSTFT, TSTFT and TDSTFT.

These transforms were derived by applying three different types of analysis windows: the original analysis window, a time ramped window, and a time derivative window, as illustrated in Fig. 6.

The proposed CTDRCepstrum (Combined Time, Time Derivative and Reassigned Cepstrum) is an innovative feature extraction method that integrates time-domain and frequency-domain reassignment analyses to effectively capture complex signal characteristics. The process is designed to enhance the accuracy of Doppler signal classification and involves the following key steps:

- Signal Preparation: The input Doppler signal is analyzed using three distinct time-domain windows:
  1. An analysis window h(t), which serves as the baseline for signal evaluation and is used for the RSTFT (Reassigned Short Time Fourier Transform) computation;
  2. A time-ramped window th(t), which emphasizes the signal's temporal progression and is used for the TSTFT (Time-Reassigned Short Time Fourier Transform) computation;
  3. A time-derivative window dh(t), which highlights rapid changes in the signal over time, used for the TDSTFT (Time Derivative-Reassigned Short Time Fourier Transform) computation.
- Short-Time Fourier Transform Reassignment (RSTFT): Each windowed signal undergoes an RSTFT, resulting in three distinct representations $STFT_{th}$, $STFT_{h}$, and $STFT_{dh}$ that capture the signal's frequency components over time through reassignment transformations;
- Corrections:
  1. Time Corrections: Applied to $STFT_{th}$ and $STFT_{h}$ to enhance temporal precision;
  2. Frequency Corrections: Applied to $STFT_{dh}$ and $STFT_{h}$ to improve frequency accuracy.
- Cepstrum of RSTFT Reassignment: The corrected signals and their respective RSTFTs are subsequently converted into the cepstral domain, which highlights the periodicity of frequency components. This process produces Cepstrumth, Cepstrumh, and Cepstrumdh, which are calculated by applying inverse RSTFTs to the logarithm of the RSTFTs;

Combining Features: The outputs from each stage are integrated into a unified feature set known as the CTDRCepstrum. This combined feature set effectively captures both the temporal and spectral characteristics of the signal through the reassignment technique, making it

highly suitable for tasks such as Doppler signal classification and pattern recognition.

4 Convolutional Neural Networks Model

Convolutional neural networks CNN is a type of deep learning algorithm that is widely used in computer vision concepts, as well as signal radar classification and object detection [30], [31], [32] and [33]. To train the CNN, the input Doppler signatures raw has been transformed into matrixes via CTDRCepstrum technique. CNN model is a mathematical construct that is involves typically composed building blocks, including the input layer, convolutional layers, pooling layers, and fully connected (FC) layers. The first two, convolution and pooling layers, perform feature extraction, whereas the third, a fully connected layer, maps the extracted features into final output, such as classification, as shown in Fig.7.

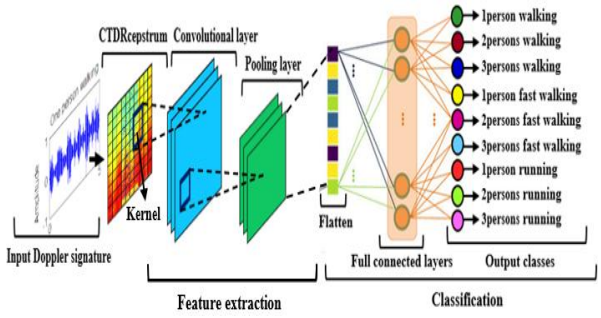

Fig. 7 1D-CNN architecture based Doppler signature.

In this research, we developed a two-dimensional CNN architecture with two convolutional and pooling layers to classify nine distinct classes. The input data consisted of nine CTDRCepstrum discriminant matrices, each measuring 257 by 60, resulting in a total size of 2313 × 60. Randomly this dataset was divided into training and testing subsets adopting any two of the three ratios: 70%-30%, 75%-25%, and 80%-20%. After splitting, the one-dimensional feature vectors were reshaped into image formats with dimensions of (height × width × channels × number of samples). For example, in the 75%-25% split, the reshaped dimensions were (60 × 1 × 1 × 1735) for training and (60 × 1 × 1 × 578) for testing. Labels were also converted into categorical format, which is compatible with the classification layer. The CNN architecture starts with an input layer designed for data of dimensions 60 × 1 × 1, followed by two convolutional layers with 32 and 64 filters, respectively, both utilizing ReLU activation functions. Each convolutional layer is succeeded by a max-pooling layer with a pool size equal to 1 × 1 and a stride equal to 1 that keeps spatial dimensions. The convolutional layers are followed by a fully connected layer with 128 neurons. The initial learning rate was set as 0.001, and the training was conducted using the Adam optimizer to determine the optimal weights (128 × 3840) and bias for the model (Table 1), minimizing the prediction cross-entropy loss. This is followed by another ReLU activation layer and a final fully connected layer with 9 neurons, corresponding to each class. The softmax activation layer with its classification layer finally provides the output.

The training progress plots generated by MATLAB R2024a are illustrated in Fig. 8, 9, and 10. The results demonstrate that a 75%-25% data split ratio yields superior performance compared to other ratios. The blue and black curves in the upper plot depict the training accuracy and validation accuracy, respectively, while the orange and black curves in the lower plot represent the training loss and validation loss. As the training iterations progressed, the accuracy curves exhibited a gradual increase, while the loss curves showed a decreasing trend. Analyzing these curves suggests that the network model achieved a good fit. Furthermore, the 75%-25% split dataset achieved an accuracy of 99.83%, confirming the model's excellent performance capabilities.

Table 1 Parameters options for training CNN.

Parameters	Value and description
Solver for training neural network	Adam (Adaptive moment estimation)
Epoch number	10
Initial Learning rate	0.001
Size of mini-batch	20
Option for data shuffling	every-epoch
Option for dropping learning rate during training	Keep learning rate constant throughout training
Factor for dropping the learning rate	0.2
Number of epochs for dropping the learning rate	10

5 Experimental Results

The aim of this study is to evaluate the effectiveness of the proposed CTDRCepstrum based Doppler signatures and enhance the classification accuracy. A series of tests and simulations using all available windows in Matlab.18.a were conducted to identify the optimal one for calculating CTDRCepstrum features. Initially, we employed the STFT reassignment based classical windows to assess the performance of the CNN classifier on the Doppler database. The results were disappointing, with accuracy rates of 77.5848% for the Rectangular window, 78.3737% for the Hanning window, and 79.5848% for the Blackman window, indicating that these windows are not suitable for feature extraction. The classification accuracy saw a notable increase with the Blackman-Harris window, reaching 84.7751%.

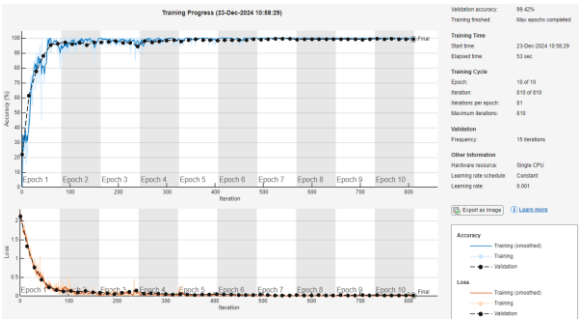

Fig. 8 Accuracy and Loss plots to display during CNN training progress using 70% training and 30% testing.

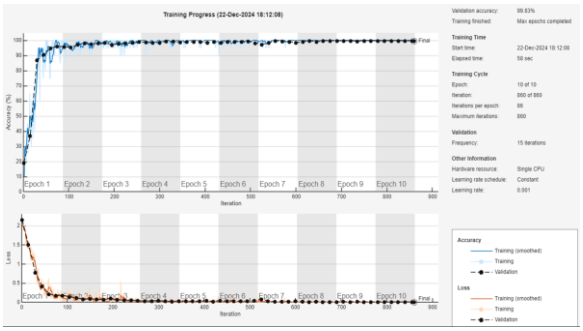

Fig. 9 Accuracy and Loss plots to display during CNN training progress using 75% training and 25% testing.

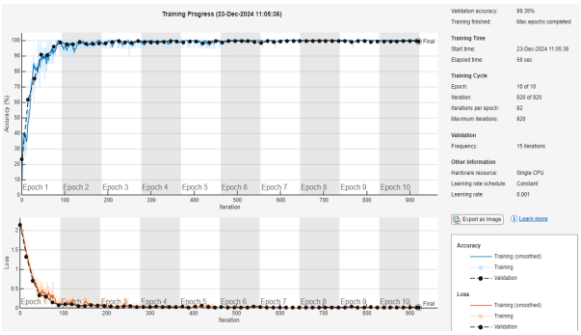

Fig. 10 Accuracy and Loss plots to display during CNN training progress using 80% training and 20% testing.

The Parzen window followed closely at 87.3702%, while the Blackman-Nuttall window achieved 87.5433%. The Nuttall window improved to 88.4083%, and the Tukey window reached 88.5813%. The HalfBand window recorded an accuracy of 88.7543%, with the Gaussian window topping the list at 90.1384%. Further enhancements in classification accuracy were observed with the Lanczos window at 91.0035%, the Flattop window at 91.8685%, Hamming at 92.3875%, and the Kaiser window at 93.2526%. The Cosine window achieved an impressive 95.1557%, while the Bartlett window reached 98.6159%. The Triangular window recorded 98.7889%, and the Bartlett-Hanning window came in at 98.9619%. These initial experiments showed that all the windows examined except for Tukey, Nuttall, Blackman-Nuttall, Parzen, and Blackman-Harris, yielded satisfactory results. The Bartlett-Hanning window is especially favored because it effectively reduces the first few side lobes while maintaining a relatively narrow main lobe width. A closer look at the results indicates that the accuracy rates alone might not be very meaningful, pointing to possible issues with performance accuracy. Thus, it is essential to apply our newly proposed CTDRCepstrum technique, which helps identify the best window for achieving the highest accuracy rates.

The experimental results demonstrated the effectiveness of our newly proposed technique, achieving impressive accuracy rates of 98.9619% with Parzen, 98.6159% with Tukey, and 98.4429% with both Hamming and Blackman-Harris. Additionally, we recorded 98.0969% with Blackman-Nuttall, 97.9239% with Blackman, 97.4048% with Hanning, 97.0588% with HalfBand, 97.0588% with Nuttall, 96.8858% with Gaussian, and 94.6367% with Rectangular window. Moreover, the CTDRCepstrum method showed a high classification accuracy of 99.8270% using the Bartlett-Hanning window, with 99.6569% for Triangular, 99.6540% for Bartlett, 99.4810% for Cosine, 99.3080% for Kaiser, and 99.1349% for both Flattop and Lanczos windows. Based on the comparison results, the CTDRCepstrum approach using the Bartlett-Hanning window, which achieved 99.8300% correct classification, outperformed all other window methods.

The performance evaluation of the CNN classification algorithm relies on the confusion matrix, which compares predicted and actual class instances. This matrix highlights the model's strengths, weaknesses, and error types by displaying predicted classes in columns and actual classes in rows. Predicted classes come from the model's estimates, while actual classes match the true observed labels. The matrix provides a clear view of correct predictions and various errors across all classes. Figures 11, 12, and 13 show confusion matrices based on different training-testing splits of the database: 70%-30%, 75%-25%, or 80%-20%.

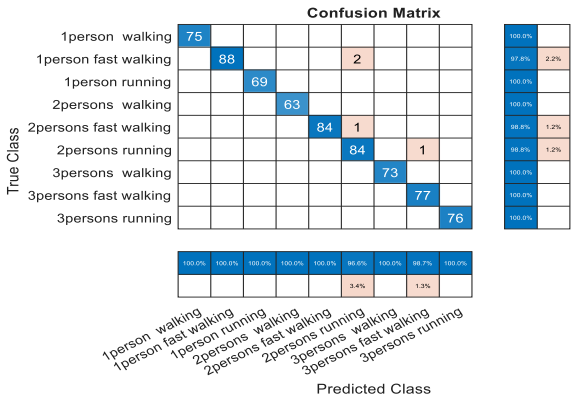

Fig. 11 Confusion matrix of 70% training and 30% testing for CNN classification using CTDRcepstrum technique based on Barttlet-Hanning window.

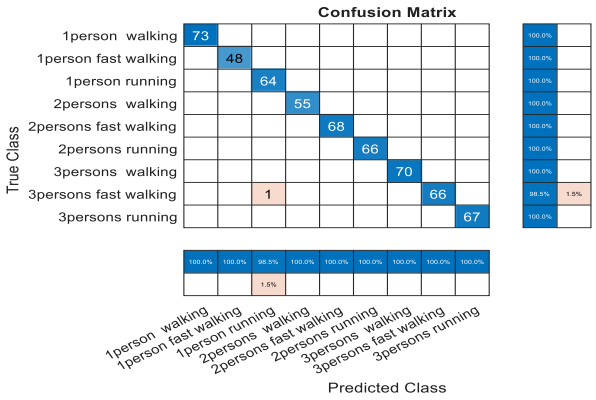

Fig. 12 Confusion matrix of 75% training and 25% testing for CNN classification using CTDRcepstrum technique based on Barttlet-Hanning window.

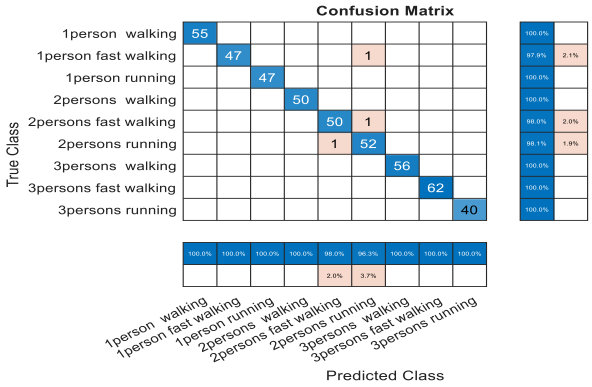

Fig. 13 Confusion matrix of 80% training and 20% testing for CNN classification using CTDRcepstrum technique based on Barttlet-Hanning window.

The evaluation of three data split ratios—70%-30%, 75%-25%, and 80%-20%—revealed distinct differences in the model's performance. Among these, the 75%-25% ratio achieved the best results, with an impressive accuracy of 99.83%. This split ratio provides an optimal balance between the amount of data used for training and testing, ensuring effective learning and robust evaluation. In contrast, the 70%-30% ratio resulted in a slightly lower accuracy of 99.42%. While this split allocates more data for testing, the reduced training data may limit the model's ability to generalize effectively, leading to a marginal decline in performance. Similarly, the 80%-20% ratio achieved an accuracy of 99.35%, the lowest among the three splits. This outcome suggests that while more training data can enhance learning, the smaller testing subset may affect the precision of performance evaluation, resulting in a minor decrease in accuracy. Overall, the results indicate that the 75%-25% split ratio is the most effective, as it ensures a balance between sufficient training data for model development and adequate testing data for robust evaluation, leading to superior classification performance.

6 Conclusion

This study presents the CTDRCepstrum, an innovative method for feature extraction designed to classify moving radar targets using Doppler signatures. The experimental results demonstrate that the CTDRCepstrum significantly enhances classification accuracy compared to conventional STFT reassignment methods. Additionally, the CTDRCepstrum, when paired with the Bartlett-Hanning window, outperforms other windowing techniques in terms of accuracy. In conclusion, the proposed CTDRCepstrum method, especially when applied with the Bartlett-Hanning window, offers substantial performance improvements over traditional windowing functions, highlighting its potential for future radar based classification applications.

Conflict of Interest

The author declares no conflict of interest.

Author Contributions

The entire study was conceived, designed, and executed by the sole author. This includes the development of the CTDRCepstrum feature extraction technique, and the application of convolutional neural networks (CNNs) for classification. The author also conducted the experimental work, interpreted the results, and wrote the manuscript. The author is solely responsible for all aspects of the work, including its accuracy and integrity.

Funding

No funding was received for this work.

Informed Consent Statement

Not applicable.

References

[1] R. Amiri, and A. Shahzadi, “Micro-Doppler based target classification in ground surveillance radar systems,” *Digital Signal Processing*, Vol. 101, pp. 102702, 2020.

[2] O. Tekir, B. Yılmaz, and C. Özdemir, “Signal preprocessing routines for the detection and classification of human micro-Doppler radar signatures,” *Microwave and Optical Technology Letters*, Vol. 65, No. 8, pp. 2132-2149, 2023.

[3] P. Cao, W. Xia, and Y. Li, “Classification of ground targets based on radar micro-Doppler signatures using deep learning and conventional supervised learning methods,” *Radioengineering*, Vol. 27, No. 3, pp. 835-845, 2018.

[4] G. Manfredi, I. D. H. Sáenz, M. Menelle, S. Saillant, J. P. Ovarlez, and L. Thirion-Lefevre,

"Measurements and analysis of the Doppler signature of a human moving within the forest in UHF-band," *Remote Sensing*, Vol. 13, No. 3, pp. 423, 2021.

[5] S. Björklund, H. Petersson, and G. Hendeby, "Features for micro-Doppler based activity classification," *IET radar, sonar & navigation*, Vol. 9, No. 9, pp. 1181-1187, 2015.

[6] S. Hassan, X. Wang, S. Ishtiaq, N. Ullah, A. Mohammad, and A. Noorwali, "Human activity classification based on dual micro-motion signatures using interferometric radar," *Remote Sensing*, Vol. 15, No. 7, pp. 1752, 2023.

[7] X. Qiao, T. Shan, R. Tao, X. Bai, and J. Zhao, "Separation of human micro-Doppler signals based on short-time fractional Fourier transform," *IEEE Sensors Journal*, Vol. 19, No. 24, pp. 12205-12216, 2019.

[8] H. T. Le, S. L. Phung, and A. Bouzerdoum, "A fast and compact deep Gabor network for micro-Doppler signal processing and human motion classification," *IEEE Sensors Journal*, Vol. 21, N. 20, pp. 23085-23097, 2021.

[9] K. Kodera, C. de Villedary, and R. Gendrin, "A new method for the numerical analysis of non-stationary signals," *Physics of the Earth and Planetary Interiors*, Vol.12, No. 142-150, pp. 142-150, 1976.

[10] F. Auger, and P. Flandrin, "Improving the readibility of time-frequency and time-scale representations by the reassignment method," *IEEE Transactions on signal processing*, Vol. 43, No. 5, pp. 1068-1089, May. 1995.

[11] I. Djurović, and LJ. Stanković, "Time–frequency representation based on the reassigned S-method," *Signal processing*, Vol. 77, No. 1, pp. 115-120, 1999.

[12] S. Hainsworth, and M. Macleod, "Time-frequency reassignment: a review and analysis," University of Cambridge, Department of Engineering, 2003.

[13] S. A. Fulop, and K. Fitz, "Algorithms for computing the time-corrected instantaneous frequency (reassigned) spectrogram, with applications," *The Journal of the Acoustical Society of America*, Vol. 119, No. 1, pp. 360-371, 2006.

[14] J. Xiao, and P. Flandrin, "Multitaper Time-Frequency Reassignment for Nonstationary Spectrum Estimation and Chirp Enhancement," *IEEE Transactions on Signal Processing*, Vol. 55, No. 6, pp. 2851-2860, Jun. 2007.

[15] L. Navarro, G. Courbebaisse, and J. C. Pinoli, "Continuous frequency and phase spectrograms: A study of their 2d and 3d capabilities and application to musical signal analysis," *Journal of Zhejiang University SCIENCE A*, Vol. 9, No. 2, pp. 199-206, 2008.

[16] S. Meignen, T. Oberlin, and S. McLaughlin, "A new algorithm for multicomponent signals analysis based on synchrosqueezing: With an application to signal sampling and denoising," *IEEE transactions on Signal Processing*, Vol. 60, No. 11, pp. 5787-5798, Nov. 2012.

[17] F. Auger, P. Flandrin, Y. T. Lin, S. McLaughlin, S. Meignen, T. Oberlin, and H. T. Wu, "Time-frequency reassignment and synchrosqueezing: An overview," *IEEE Signal Processing Magazine*, Vol. 30, No. 6, pp. 32-41, Nov. 2013.

[18] A. Ahrabian, and D. P. Mandic, "Selective Time-Frequency Reassignment Based on Synchrosqueezing," *IEEE Signal Processing Letters*, Vol. 22, No. 11, pp. 2039-2043, Nov. 2015.

[19] D. L. Stevens, and S. A. Schuckers, "Analysis of Low Probability of Intercept Radar Signals Using the Reassignment Method," *American Journal of Engineering and Applied Sciences*, Vol. 8, No. 1, pp. 26, 2015.

[20] G. Manfredi, I. D. Hinostroza Sáenz, M. Menelle, S. Saillant, J. P. Ovarlez, and L. Thirion-Lefevre, "Time-frequency characterisation of bistatic Doppler signature of a wooded area walk at L-band," *IET Radar, Sonar & Navigation*, Vol. 15, No. 12, pp. 1573-1582, 2021.

[21] P. Flandrin, F. Auger, and E. Chassande-Mottin. "Time-Frequency reassignment: From principles to algorithms," *In Applications in Time-Frequency Signal Processing*, CRC Press, pp. 179-204, 2018.

[22] D. He, H. Cao, S. Wang, and X. Chen, "Time-reassigned synchrosqueezing transform: the algorithm and its applications in mechanical signal processing," *Mechanical Systems and Signal Processing*, Vol. 117, pp. 255-279, 2019.

[23] Z. He, X. Tu, W. Bao, Y. Hu, and F. Li, "Gaussian-modulated linear group delay model: application to second-order time-reassigned synchrosqueezing transform," *Signal Processing*, Vol. 167, pp. 107275, 2020.

[24] X. Tu, Q. Zhang, Z. He, Y. Hu, S. Abbas, and F. Li, "Generalized horizontal synchrosqueezing transform: Algorithm and applications," *IEEE Transactions on Industrial Electronics*, V. 68, No. 6, pp. 5293-5303, 2021.

[25] F. L´eonard, "Phase spectrogramand frequency spectrogram as new diagnostic tools," *Mechanical Systems and Signal Processing*, Vol. 21, No. 1, pp. 125-137, 2007.

[26] L. Navarro, G. Courbebaisse. and J. C. Pinoli, "Continuous frequency and phase spectrograms: A study of their 2d and 3d capabilities and application to musical signal analysis," *Journal of Zhejiang University SCIENCE A*, Vol. 9, No. 2, pp. 199-206, 2008.
[27] V. Bruni, M. Tartaglione, and D. Vitulano, "A Fast and Robust Spectrogram Reassignment Method," *Mathematics*, Vol.7. No. 4, pp. 358, 2019.
[28] S. A. Samad, and A. B. Huddin, "Improving spectrogram correlation filters with time-frequency reassignment for bio-acoustic signal classification," *Indonesian Journal of Electrical Engineering and Computer Science*, Vol.14, No. 1, pp. 62-67, April. 2019.
[29] V. C. Chen, and S. Qian, "Joint time-frequency transform for radar range-Doppler imaging," *IEEE transactions on aerospace and electronic systems*, Vol. 34, No. 2, pp. 486-499, 1998.
[30] Z. Li, F. Liu, W. Yang, S. Peng, and J. Zhou, "A survey of convolutional neural networks: analysis, applications, and prospects," *IEEE transactions on neural networks and learning systems*, Vol. 33, No. 12, pp. 6999-7019, 2021.
[31] Y. Kim, I. Alnujaim, S. You, and B. J. Jeong, "Human detection based on time-varying signature on range-Doppler diagram using deep neural networks," *IEEE Geoscience and Remote Sensing Letters*, Vol. 18, No. 3, pp. 426-430, 2020.
[32] M. K. Ha, T. L. Phan, D. H. H. Nguyen, N. H. Quan, N. Q. Ha-Phan, C. T. S. Ching, and N. V. Hieu, "Comparative Analysis of Audio Processing Techniques on Doppler Radar Signature of Human Walking Motion Using CNN Models," *Sensors*, Vol. 23, No. 21, pp. 8743, 2023.
[33] D. Buchman, M. Drozdov, T. Krilavičius, R. Maskeliūnas, and R. Damaševičius, "Pedestrian and animal recognition using doppler radar signature and deep learning," *Sensors*, Vol. 22, No. 9, pp. 3456, 2022.

Dr. Dalila Yessad was born in 1978 in Mila, Algeria. She received her State Engineer's diploma in electronics from Jijel University in 2002. She completed her Master's degree in electronics, specializing in advanced signal processing techniques, at the Military Polytechnic School (EMP) in Algiers in 2009.

In 2014, she obtained her PhD in electronics, focusing on spoken communication, from the University of Sciences and Technology Houari Boumediene (USTHB) in Algiers. Currently, she is a lecturer in the Department of Electromechanical and Mechanical Engineering at Mila University. She is also a member of the Laboratoire d′Analyse des Signaux et Systèmes at Mohamed Boudiaf University of M'sila. Her research interests include biometric recognition, signal processing, speech and speaker recognition, Doppler radar, solar energy, instrumentation and measurement, PID regulation, Arduino, smart sensors, and artificial intelligence.